REVIEW ON PHYSICS OF $e^+e^- \to t\bar{t}$ NEAR THRESHOLD*

Y. SUMINO

Department of Physics, Tohoku University
Sendai, 980 Japan

(Received November 3, 1994)

We review the recent developments of studies on $e^+e^- \to t\bar{t}$ in the threshold region. It has been shown that the top threshold cross sections will be able to provide many important and interesting physics. Due to the large mass and the large decay width of top quark, there will appear a number of unique features at top threshold. First, theoretical background is summarized. Then we present observables that are typical to the top threshold region, and discuss the physics that can be extracted. Also, we list the results of the recent parameter determination study taking a sample case of $m_t = 170$ GeV.

PACS numbers: 13.65. +i

1. Introduction

We review the physics of $e^+e^- \to t\bar{t} \to t\bar{t}$ near threshold ($E_{c.m.} \simeq 2m_t$) in this paper. In the beginning let us briefly comment on the role of future $e^+e^- \to t\bar{t}$ colliders in order to give some idea to the readers on the status of future top quark physics from a more general viewpoint.

1.1. About NLC

It has recently been recognized that a next generation linear $e^+e^- \to t\bar{t}$ collider (NLC), with energy accessible up to $\sim$ 500 GeV in its first stage operation, will be able to provide important contributions to future elementary particle physics field [1]. Possibility to build such a collider is now seriously considered at KEK, DESY, and SLAC. These machines aim at

---

* Presented at the XXXIV Cracow School of Theoretical Physics, Zakopane, Poland, June 1–10, 1994.

the luminosity of 10^{33}-10^{34} $\mathrm{cm}^{-2}\mathrm{sec}^{-1}$, which corresponds to 10^5-10^6 W's and 10^3-10^4 top quarks produced per year assuming the standard model cross sections. Also, due to the characteristics of linear colliders, the beam energy will be adjustable downward within a range of a few hundred GeV, a highly longitudinally polarized electron beam can be used, etc.

NLC will be designed so that it can test the standard model predictions with good accuracy at the energy approximating the electroweak symmetry breaking scale. Therefore, one may address the aim of NLC as the investigation of electroweak symmetry breaking physics and the search for any new physics to appear. Target particles necessarily are W and Z, Higgs particle and top quark, and not to mention non-standard-model particles if any. As the W and Z are massive, we know their longitudinal components come from the electroweak symmetry breaking sector, and we may extract information on it from detailed studies of the properties of the gauge bosons. The Higgs is the very particle that is responsible for the symmetry breaking mechanism within the standard model (and also in many of its extensions) so that its discovery and/or the detailed study of its properties will be crucial in understanding the fundamental physics. The top quark is the heaviest fermion in the standard model with the mass of the order of the electroweak symmetry breaking scale, and one may again expect to probe the symmetry breaking physics using top quark.

In the rest of this paper we focus on the physics that can be extracted through the study of top quark pair production process near threshold at NLC. It turns out that the study of top quark threshold is quite promising and also very interesting among the various subjects of NLC. The threshold cross section depends on physical parameters such as top mass m_t, strong coupling constant α_s, top width Γ_t, Higgs mass M_H, top-Higgs Yukawa coupling g_tH, *etc.*, as we will see in the following.

1.2. What do we expect at top threshold?

As compared to all other fermions, two of the unique properties of top quark are that it is extremely heavy and that it has very short lifetime. CDF group has recently announced the evidence for $\mathrm{t\bar{t}}$ production [2], and the reported top quark mass

$$m_\mathrm{t} = 174 \pm 10^{+13}_{-12}\ \mathrm{GeV} \tag{1.1}$$

agrees very well with the indirect determination from the LEP and SLAC data [3]. The top quark decays almost 100% to b quark and W within the standard model. The decay width of top quark Γ_t is predictable as a function of m_t, and already fairly precise theoretical prediction at the level of a few percent accuracy is available [4]. Here, we note that $\Gamma_\mathrm{t} \sim 1$ GeV for the relevant top quark mass.

Near the threshold of top quark pair production one might expect the formation of $t\bar{t}$ resonances. Along with the resonance formation, cross section gets enhanced by QCD interaction. Produced t and $\bar{t}$, however, decay quickly via electroweak interaction and the enhancement is reduced accordingly. In fact there will appear subtle interplays between QCD and electroweak interactions.

Consider the time evolution of the $t\bar{t}$ pair produced in $e^+e^- \to t\bar{t}$ annihilation as they spread apart from each other (Fig. 1). Since they are slow near the threshold, they cannot escape even relatively weak attractive force mediated by the exchange of Coulomb gluons; t and $\bar{t}$ are bound to form the Coulombic resonances when they reach the distance of Bohr radius $(\alpha_s m_t)^{-1} \sim 0.1\ \mathrm{GeV}^{-1}$. At this stage, the coupling of top quark to gluon is of the order of $\alpha_s(\mu = \alpha_s m_t) \sim 0.15$. If they could continue to spread apart even further to the distance $\Lambda_{\mathrm{QCD}}^{-1} \sim$ a few GeV^{-1}, there would occur the hadronization effect as the coupling becomes really strong, since gluons with wave-length $\sim \Lambda_{\mathrm{QCD}}^{-1}$ would be able to resolve the color charge of each constituent. For a realistic top quark, however, the $t\bar{t}$ pair will decay at the distance $(m_t \Gamma_t)^{-1/2} \sim 0.1\ \mathrm{GeV}^{-1}$ into energetic b and $\bar{b}$ jets and W's before the hadronization effect becomes important. Here, the toponium can be regarded as the Coulombic resonance state (with reasonably weak coupling) due to the large mass and width of top quark. In this respect, the toponium resonances differ distinctly from the charmonium and bottomonium resonances which have smaller masses as well as narrow widths. Besides, since the toponium resonances decay dominantly via electroweak interaction [5, 6], their decay process can also be calculated reliably.

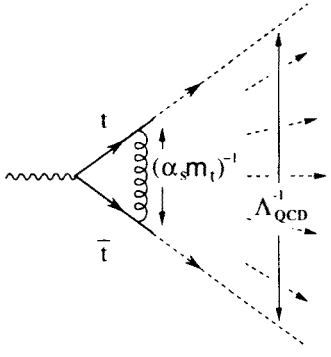

Fig. 1. Top quark pair production near threshold. Top quark will decay before hadronization occurs.

The distinct resonance shape of the total cross section that would appear for narrow resonances gets smeared due to large top quark width, merging into a broad enhancement of the cross section over the threshold

region (see Fig. 6.a.). Generally, the QCD enhancement is still large enough to allow precise test of QCD in the $t\bar{t}$ threshold region, but one is obliged to study the overall shape of the total cross section instead of applying the spectroscopic method developed at charmonium and bottomonium resonances [7, 8]. Besides total cross section there are two other observables that are unique to the $t\bar{t}$ threshold region. It was pointed out that through the measurement of top quark momentum distribution in the threshold region one can extract information on the QCD binding effect independent of that from the total cross section [9, 10]. Also there will appear observable forward-backward (FB) asymmetry of top quark even below threshold, which provides yet another independent information of the toponium resonances [11].

In Section 2, we review the basic theoretical aspects of $t\bar{t}$ threshold which allow for reliable estimates of cross sections. In Section 3, we present various observables at $t\bar{t}$ threshold, and discuss the physics that can be extracted. Section 4 lists the results of the recent parameter determination study from the $t\bar{t}$ threshold cross sections. Concluding remarks are given in Section 5.

2. Theoretical background

Fadin and Khoze first pointed out that the top quark threshold cross section will provide a very clean test of QCD since fairly stable theoretical prediction is available [7]. First, the large top quark mass enables the probe of asymptotic region ($\mu \gtrsim 10$ GeV) of QCD where the theoretical control is more feasible. Secondly, the large width of top quark will act as the infrared cutoff which prevents the hadronization effects to affect the cross section. Thirdly, space like region of gluon momentum plays the prime role in the QCD enhancement.

In this section we will review the basic theoretical concept necessary for dealing with the threshold bound states. We see that non-perturbative yet systematic discussion is possible. The upshot is that the $t\bar{t}$ production vertex can be calculated in terms of the Green function of the non-relativistic Schrödinger equation [7].

2.1. Leading threshold singularities

It is well-known that near the threshold of quark-antiquark ($q\bar{q}$) pair production, naive perturbation theory breaks down due to the formation of bound states [12, 13]. Intuitively, this is because the produced q and $\bar{q}$ have small velocities so that they are trapped by the attractive force mediated by the exchange of gluons. Thus, multiple exchange of gluons becomes

more significant and the strong interaction is enhanced accordingly. We will briefly review this property near $t\bar{t}$ threshold. We demonstrate explicitly that the ladder diagrams exhibit the gauge-invariant leading singularities. In this subsection, we neglect the decay of t and $\bar{t}$, and treat them as stable particles.

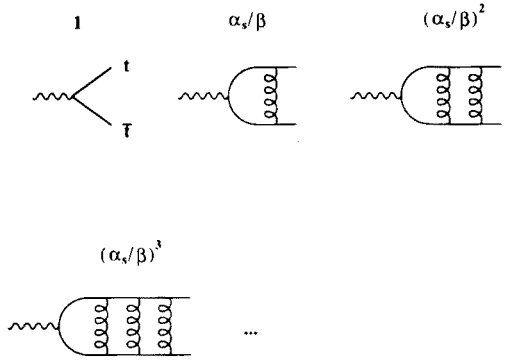

Fig. 2. The ladder diagrams for the process $\gamma^* \to t\bar{t}$. The diagram where n uncrossed gluons are exchanged has the behavior $\sim (\alpha_s/\beta)^n$ near threshold.

Let us consider the amplitude where a virtual photon decays into t and $\bar{t}$, $\gamma^* \to t\bar{t}$, just above the threshold of $t\bar{t}$ pair production. As we will see below, the ladder diagram for this process where uncrossed gluons are exchanged n times between t and $\bar{t}$ has the behavior $\sim (\alpha_s/\beta)^n$, see Fig. 2. Here, β is the velocity of t or $\bar{t}$ in the c.m. frame,

$$\beta = \sqrt{1 - \frac{4m_t^2}{s}}\,. \tag{2.2}$$

Hence, the contribution of the n-th ladder diagram will not be small even for large n if $\beta \lesssim \alpha_s$. That is, the higher order terms in α_s remain unsuppressed in the threshold region. The singularities which appear at this specific kinematical configuration is known as "threshold singularities"[1].

We may observe the appearance of $\sim (\alpha_s/\beta)^n$ in the n-th ladder diagram as follows.

First, consider the one-loop diagram. Its *imaginary* part can be estimated using the Cutkosky rule (cut-diagram method), see Fig. 3. Namely, the imaginary part is given by the phase space integration of the product of the tree diagrams. The intermediate $t\bar{t}$ phase space is proportional to β as

$$d\Phi_2(t\bar{t}) = \frac{\beta}{16\pi}\, d\cos\theta\,, \tag{2.3}$$

[1] This singularity stems from the fact that, for a particular assignment of the loop momenta, all the internal particles can become very nearly on-shell simultaneously as $\beta \to 0$.

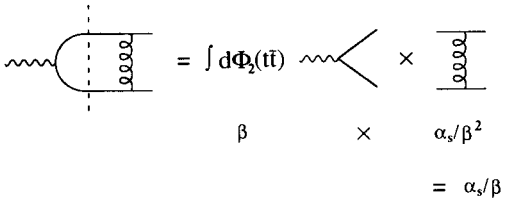

Fig. 3. The Cutkosky rule for evaluating the imaginary part of the 1-loop diagram. The factors in α_s and β are shown explicitly.

where θ is the angle between the momenta of the intermediate top quark and the final top quark in the c.m. frame. Meanwhile the $t\bar{t}$ scattering diagram with t-channel gluon exchange contributes the factor $\sim \alpha_s/\beta^2$ since the gluon propagator is proportional to $1/\beta^2$. In fact the propagator denominator is given by

$$k^2 = -\boldsymbol{k}^2 = -\frac{s\beta^2}{2}(1-\cos\theta)\,, \tag{2.4}$$

where $k \propto \beta$ denotes the gluon momentum.

Thus, we see that the imaginary part of the one-loop diagram has the behavior $\sim \beta \times \alpha_s/\beta^2 = \alpha_s/\beta$. By repeatedly using the cut-diagram method, one can induce that the imaginary part of the ladder diagram with n uncrossed gluons has the behavior $\sim (\alpha_s/\beta)^n$, see Fig. 4.

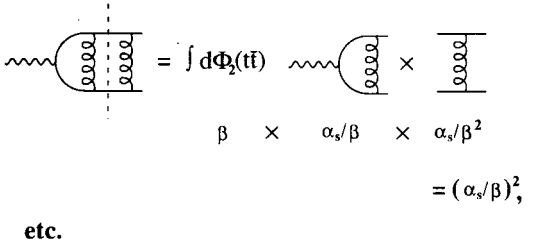

Fig. 4. The cut-diagram method for evaluating the singularities of the higher order ladder diagrams. The factors in α_s and β are shown explicitly.

Note that the leading part of the gluon propagator in powers of β (in R_ξ-gauge) is the instantaneous (Coulomb) propagator as

$$\bar{u}_f\gamma^\mu u_I \frac{-i}{k^2+i\varepsilon}\left[g_{\mu\nu}-(1-\xi)\frac{k_\mu k_\nu}{k^2}\right]\bar{v}_I\gamma^\nu v_f \to \bar{u}_f\gamma^0 u_I\,\frac{-i}{-\boldsymbol{k}^2+i\varepsilon}\bar{v}_I\gamma^0 v_f\,. \tag{2.5}$$

Here, the subscripts f and I stand for the final state and the intermediate state, respectively. We used the fact that the space components of the currents, $\bar{u}_f \gamma^\mu u_I$ and $\bar{v}_I \gamma^\nu v_f$, are order β in the c.m. frame [2].

It can be checked by power counting method [14] that the *real* part of the n-th ladder diagram exhibits the same type of singularity, $\sim (\alpha_s/\beta)^n$. The relevant loop momenta in the loop integrals are also in the non-relativistic regime:

$$p_t^0 - m_t, \bar{p}_t^0 - m_t \sim O(\beta^2), \qquad \boldsymbol{p}_t = -\bar{\boldsymbol{p}}_t \sim O(\beta), \tag{2.6}$$

$$k^0 \sim O(\beta^2), \qquad \boldsymbol{k} \sim O(\beta). \tag{2.7}$$

Here, p_t, $\bar{p}_t$ and k represent the internal momenta of t, $\bar{t}$ and the gluon, respectively, in the c.m. frame. It is easy to see that, for such configurations, $t(\bar{t})$ and gluon propagators are counted as $\sim 1/\beta^2$, and the measure for the each loop integration $d^4k/(2\pi)^4$ as $\sim \beta^5$.

Thus, the ladder diagrams exhibit the leading singularities $\sim (\alpha_s/\beta)^n$. Other diagrams, including crossed gluon diagrams, do not exhibit the leading singularities, but contribute to the non-leading singularities $\sim \alpha_s^{n+l}/\beta^n$ $(l \geq 1)$.

One may worry about the gauge invariance of the amplitude if we take only the ladder diagrams. Let us write the amplitude for the process $e^+e^- \to t\bar{t}$ with full QCD corrections near threshold as

$$M^{(\mathrm{full})}(\alpha_s, \beta) = \sum_n c_n (\alpha_s/\beta)^n + (\text{non-leading terms}). \tag{2.8}$$

Then the coefficients c_n's should be gauge-independent since the full QCD amplitude $M^{(\mathrm{full})}$ is gauge invariant. (We suppressed the variables other than α_s and β.) Explicitly, the gauge-independence of c_n's is ensured by the gauge-independence of the leading part $\sim 1/\beta^2$ of the gluon propagator in Eq. (2.5).

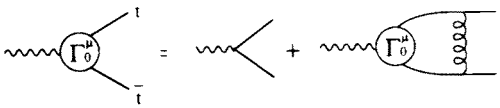

Fig. 5. The self-consistent equation satisfied by the leading singularities of the $t\bar{t}\gamma$ vertex Γ_0^μ. One should take only the leading part $\sim (\alpha_s/\beta)^n$ on both sides of the equation.

[2] Dirac representation of the γ-matrices is most useful in understanding the power count, where γ^0 is diagonal and γ^i's are off-diagonal. The t-quark spinor wave function has the upper two components with order of unity and the lower two components suppressed by β, and vice versa for the $\bar{t}$-quark.

As the higher order terms in α_s can no longer be neglected near threshold, we are led to sum over the leading threshold singularities. Let us denote by Γ_0^μ the leading singularities of the vertex $\gamma^* \to t\bar{t}$, which satisfies the self-consistent equation as depicted in Fig. 5. By taking only the leading part $\sim (\alpha_s/\beta)^n$ on both sides of the equation, one obtains[3] the vertex Γ_0^μ as

$$\Gamma_0^\mu = -\left(\frac{1+\gamma^0}{2}\gamma^\mu\frac{1-\gamma^0}{2}\right)(E - \boldsymbol{p}_t^2/m_t)\,\tilde{G}_0(\boldsymbol{p}_t; E)\,, \tag{2.9}$$

where $E = \sqrt{s} - 2m_t$ is the energy measured from the threshold. $\tilde{G}_0(\boldsymbol{p}; E)$ is the S-wave Green's function of the non-relativistic Schrödinger equation with Coulomb potential:

$$\left[\left(-\frac{\nabla^2}{m_t} + V(r)\right) - (E + i\varepsilon)\right] G_0(\boldsymbol{x}; E) = \delta^3(\boldsymbol{x})\,, \tag{2.10}$$

$$\tilde{G}_0(\boldsymbol{p}; E) = \int d^3\boldsymbol{x} e^{-i\boldsymbol{p}\cdot\boldsymbol{x}}\, G_0(\boldsymbol{x}; E)\,, \tag{2.11}$$

$$V(r) = -C_F\frac{\alpha_s}{r}\,, \tag{2.12}$$

where $C_F = 4/3$ is the color factor. Explicitly, we may write

$$\tilde{G}_0(\boldsymbol{p}; E) = -\sum_n \frac{\phi_n(\boldsymbol{p})\psi_n^*(\boldsymbol{0})}{E - E_n + i\varepsilon}\,, \tag{2.13}$$

where $\phi_n(\boldsymbol{p})$ and $\psi_n(\boldsymbol{x})$ are the Coulomb wave functions in momentum space and coordinate space, respectively. Here, n includes the bound states, $E_n = -(C_F\alpha_s)^2 m_t/4n^2$, and continuum states for $E_n > 0$. Only the S-wave states contribute to the leading vertex as seen from the appearance of $\psi_n(\boldsymbol{0})$[4].

As for the amplitude for $e^+e^- \to t\bar{t}$ near threshold, one may take the leading singularities $\Gamma_0^\mu = \sum c_n^{(0)}(\alpha_s^n/\beta^n)$ as the zeroth order of the new perturbative expansion, and consider $\Gamma_1^\mu = \sum c_n^{(1)}(\alpha_s^{n+1}/\beta^n)$, $\Gamma_2^\mu = \sum c_n^{(2)}(\alpha_s^{n+2}/\beta^n)$, ..., as the higher order corrections. They are gauge invariant at each order. One may regard Γ_1^μ as $O(\alpha_s)$ or $O(\beta)$ correction to the zeroth order Γ_0^μ, since $\alpha_s^{n+1}/\beta^n = \alpha_s(\alpha_s/\beta)^n = \beta(\alpha_s/\beta)^{n+1}$ [5]. Note

[3] See, for example, Ref. [8] for a fairly systematic derivation of the vertex Γ_0^μ.

[4] To see that $(E - p^2/m_t)\tilde{G}_0(p; E)$ is a function of α_s/β, one should identify $E \to m_t\beta^2$ and $|\boldsymbol{p}| \to m_t\beta$ in the leading order.

[5] More rigorously, one should reorganize the perturbative expansion so as to include higher order corrections to the resonance mass, the residue of the resonance pole, etc. See Ref. [15] for the detail.

that the expansion parameter β is guaranteed to be small if α_s is small, since we are interested in the summation of the leading singularities only in the kinematical region where the naive perturbation theory breaks down ($\beta \lesssim \alpha_s$).

Near the $t\bar{t}$ threshold, α_s will be order 10% , and the above new expansion will be justifiable. It is important to include the $O(\alpha_s) = O(\beta)$ corrections to the cross sections for practical purposes. (See subsection 3.e.)

2.2. Top width as IR cutoff

The discussion of the leading threshold singularities in the previous subsection is identical to that of QED bound states such as positronium. In QCD, however, one would expect additional non-perturbative effects arising from the infrared region of gluon momentum. As seen in Eq. (2.4), the typical gluon momentum scale involved in the formation of bound states is $k^2 \sim -2m_t^2\beta^2$. It may even become zero at the threshold, $s = 4m_t^2$.

One can show using the spectral representation of top propagator that, if we include the large decay width of top quark, the gluon momentum scale will be effectively cut off as

$$|k^2| \gtrsim 2m_t\Gamma_t\,, \tag{2.14}$$

and the singular behavior in the amplitude is avoided [15]. At the leading order approximation, the effect of top quark width is accounted for by replacing $E \to E + i\Gamma_t$ in Eqs (2.9) and (2.10) [7]. For instance, $\sqrt{2m_t\Gamma_t} \simeq 24$ GeV for $m_t = 180$ GeV. (See subsection 1.b.)

3. Cross sections near $t\bar{t}$ threshold

In this section analyses of the cross sections in the $t\bar{t}$ threshold region are presented. There are three independent observables typical to the top quark threshold, namely, total cross section, top momentum distribution and FB-asymmetry of top quark. We discuss the physics that can be extracted from these observables.

3.1. Total cross section

The total cross section in the $t\bar{t}$ threshold region can be obtained from the leading $t\bar{t}$ production vertex (2.9) and its higher order correction. Using the optical theorem, one finds

$$\begin{aligned}\sigma_{\rm tot} &= \sigma_{t\bar{t}}(\sqrt{s}, m_t, \alpha_s, \Gamma_t, M_H, g_{tH}) \\ &\propto \mathrm{Im}\, G(\boldsymbol{x} = 0; E) \simeq -\mathrm{Im} \sum_n \frac{|\psi_n(\mathbf{0})|^2}{E - E_n + i\Gamma_t}\,.\end{aligned} \tag{3.15}$$

It is dependent on various physical parameters [7, 8] [6]. The denominator shows the resonance structure, but due to the large width Γ_t, the detail of the structure is smeared out. The normalization of the cross section is

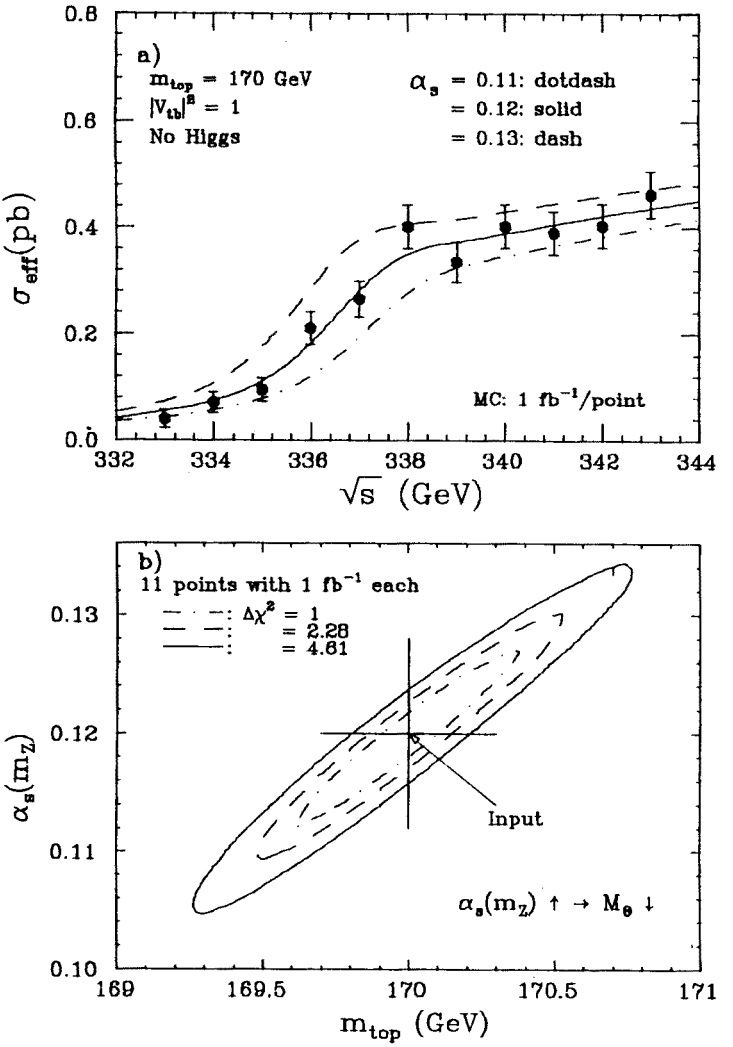

Fig. 6. (a) An example of energy scan to determine m_t and $\alpha_s(m_Z)$ where each point corresponds to 1 fb^{-1}. (b) The contour resulting from the fit to the data points [16].

---

[6] Although Γ_t can be calculated from m_t in the standard model, this relation deviates with simple extensions of the model. *e.g.* $\Gamma_t \propto |V_{tb}|^2$ can be smaller if there is a fourth generation, whereas it will be greater if there are additional decay modes such as $t \to bH^+$ or $t \to \tilde{t}\tilde{\chi}$. Thus, it is important to measure Γ_t.

determined by the wave function at the origin, which is affected by the QCD binding effect.

A sample analysis is given in Fig. 6. Three lines in Fig 6.a correspond to different values of $\alpha_s(m_Z)$. As α_s is increased the shoulder of the cross section moves to the left due to the increase of the binding energy. The normalization of the cross section is enhanced at the same time. From the fit of the theoretical prediction to the Monte Carlo events, $\alpha_s(m_Z)$ and m_t are determined in Fig 6.b.

3.2. Top momentum distribution

Besides total cross section, one can measure the momentum distribution of top quark in the threshold region by reconstructing the top quark momentum $\boldsymbol{p}$ from the final bW jet momenta [18]. Both 6-jet mode and lepton-plus-4-jet mode can be used to reconstruct the top momentum. The top quark momentum distribution in the leading order is proportional to the square of the Green function [9, 10],

$$\frac{d\sigma}{d|\boldsymbol{p}|} \propto |\tilde{G}(\boldsymbol{p}; E)|^2 \simeq \left| \sum_n \frac{\phi_n(\boldsymbol{p})\psi_n^*(\boldsymbol{0})}{E - E_n + i\Gamma_t} \right|^2 . \tag{3.16}$$

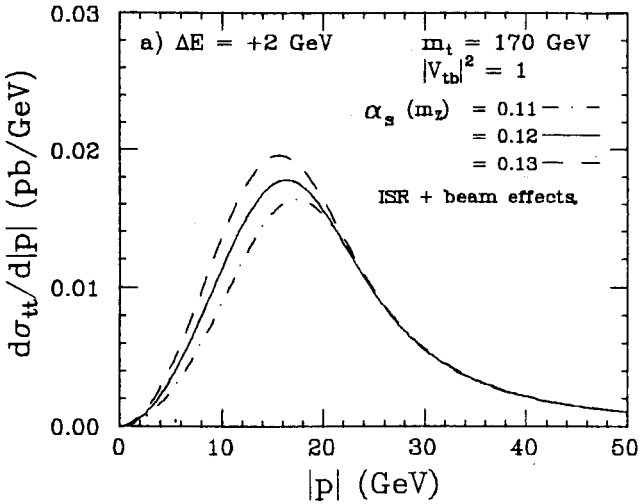

Fig. 7. The top momentum distribution at the c.m. energy 2 GeV above the first peak, $\Delta E = E - E_{1S} = 2$ GeV, for $\alpha_s(m_Z) = 0.11$, 0.12, and 0.13 with $m_t = 170$ GeV [16].

Therefore, we may measure the momentum space wave functions of toponium resonances using top quark momentum distribution. Thus, the momentum distribution provides information independent of that from the total cross section, so that it can be used to measure physical parameters ($\alpha_s, m_t, |V_{tb}|^2$, *etc.*) efficiently near threshold. Fig. 7 shows the top momentum distribution for three values of $\alpha_s(m_Z)$. The peak position of the distribution turns out to be a most suitable observable [18].

For instance, the errors on $\alpha_s(m_Z)$ and m_t (statistical only) are estimated to be reduced to about 60% through the simultaneous measurements of the total cross section and momentum distribution as compared to those determined from the total cross section alone [19].

3.3. Higgs effects

Perhaps Higgs effects are especially interesting.

If the Higgs particle turns out to be light ($M_H \lesssim 100$ GeV), there is a chance to extract the Yukawa coupling of top quark. Formalism for including Higgs effect has been developed in Ref. [20]. Qualitatively, the effect of Higgs exchange between t and $\bar{t}$ can be understood as including the Yukawa potential

$$V_{\mathrm{Yuk}}(r) = -\frac{g_{tH}^2}{4\pi}\frac{\mathrm{e}^{-M_H r}}{r} \tag{3.17}$$

into the Schrödinger equation (2.10). The effect is larger for smaller M_H and larger g_{tH}. Note that the Higgs mass should not be taken as a parameter, since if the Higgs effect is of observable size, it will already have been found at NLC and M_H will have been determined [1].

As the Yukawa potential is much short-ranged compared to the toponium resonance size, it does not affect the resonance spectra but makes the wave function at the origin significantly larger. Thus, only the normalization of the total cross section is changed, while the momentum distribution of top quark is quite insensitive to the Yukawa coupling. Fig. 8 demonstrates the dependence of the total cross section on M_H and g_{tH}.

If Higgs particle turns out to be heavier than $\sim$ 400 GeV, it is likely that a 500 GeV NLC cannot observe it. In such a case, one may still be able to predict the Higgs mass through loop effects. Although the Higgs mass dependences of the loop effects are small, using the interrelation among the precisely determined top quark mass, the final data of LEP I, the direct W mass measurements, and left-right asymmetry for polarized electron beams, we may guess the next energy region to search for Higgs. See Fig. 9.

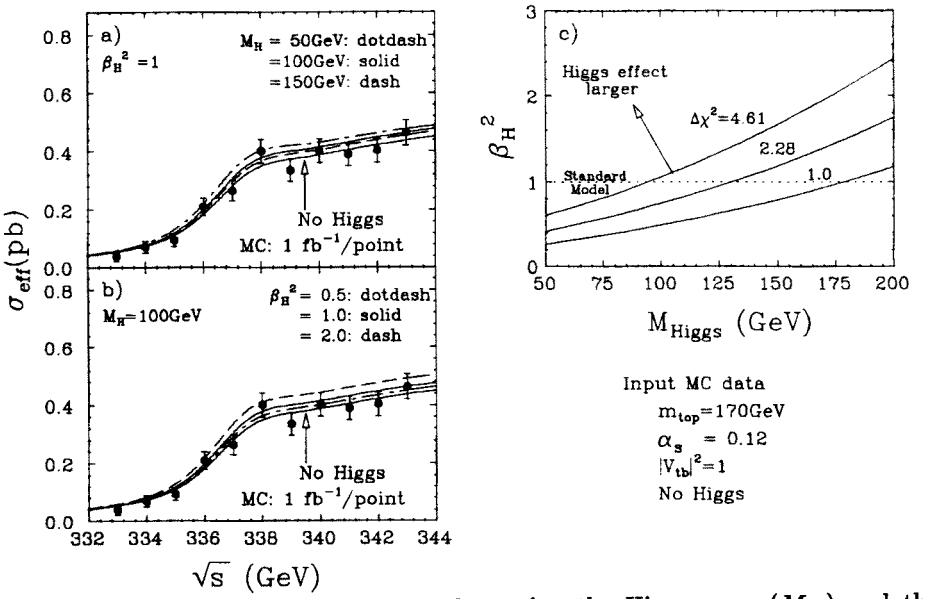

Fig. 8. An example of energy scan to determine the Higgs mass (M_H) and the normalized top-Higgs Yukawa coupling ($\beta_H = g_{tH}/g_{tH}^{SM}$) where the cross section curves are superimposed for several M_H values. (b) The same plot with the cross section curves for several β_H^2 values. (c) The contour resulting from the fit to the data points [16].

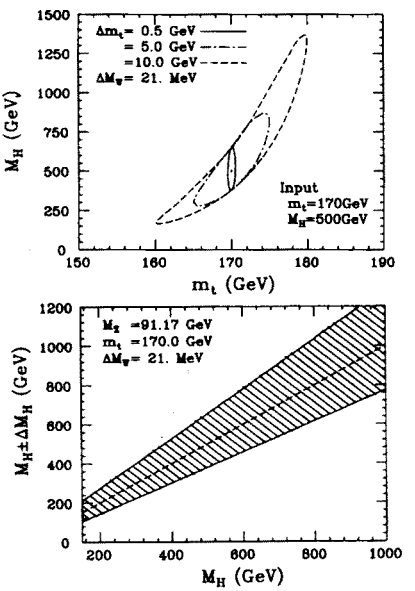

Fig. 9. (a) The 1-σ contours in the m_t-M_H plane for ΔM_W = 21 MeV and Δm_t = 0.5, 5.0, and 10.0 GeV. The bounds on Higgs mass quickly shrink with the increasing accuracy of m_t. Input values are m_t = 170 GeV and M_H = 500 GeV. (b) The 1-σ bounds on the Higgs mass as a function of the input Higgs mass when we assume ΔM_W = 21 MeV and Δm_t = 0.5 GeV [17].

3.4. *Forward–backward asymmetry of top*

One of the unique features of toponium resonances is the appearance of observable FB-asymmetry of top quark in the threshold region. The main contribution to the FB-asymmetry stems from the interference of the vector and axial-vector vertices [11, 15].

In the $e^+e^- \to t\bar{t}$ process, one can show from the spin-parity argument that the $t\bar{t}V$ ($V = \gamma, Z$) vector vertex creates S and D-wave resonance states, while the $t\bar{t}Z$ axial-vector vertex creates P-wave states. Since the P-wave amplitude is suppressed by a power of β near threshold, its interference with S-wave resonance states gives rise to the order β correction to the leading S-wave contribution to the cross sections. Since the interference term of the vector and axial-vector couplings is proportional to $\cos\theta$, $S-P$ interference produces the FB-asymmetry at $O(\beta)$.

In general, S-wave resonance states and P-wave resonance states have different energy spectra. So if the c.m. energy is fixed at either of the spectrum, there would be no contribution from the other. However, the widths of resonances grow rapidly as m_t increases, and they become so large that S-wave and P-wave resonance states start to interfere for $m_t \gtrsim 100$ GeV. This gives rise to the FB-asymmetry even below threshold, and provides

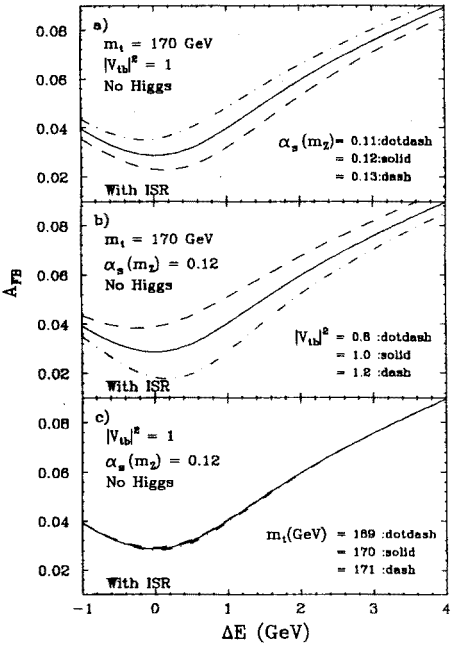

Fig. 10. The forward-backward asymmetry of top quark as a function of the energy measured from the first peak, $\Delta E = E - E_{1S}$, showing the dependence on (a) $\alpha_s(m_Z)$, (b) $|V_{tb}|^2 = \Gamma_t/\Gamma_t^{SM}$, and (c) m_t [16].

information on the resonance level structure which is concealed in the total cross section due to the large smearing effect.

In Fig. 10 we show the FB-asymmetry as a function of energy measured from the 1S resonance mass, $\Delta E = E - E_{1S}$. One sees that the asymmetry increases up to the 10% level as the energy is raised. This is because the energy levels of the resonances appear closer to one another for larger E, and the overlap of the S and P-wave states become more severe. Note the α_s-dependence of the FB-asymmetry: the asymmetry decreases as α_s is raised. This is because the resonance levels spread apart from each other with the growth of binding energy, and also because the $O(\alpha_s)$ correction of the top quark width reduces the width for larger α_s.

So, in essence, the FB-asymmetry "measures" the degree of overlap of S-wave and P-wave resonances.

3.5. Effects of next-to-leading order corrections

As discussed in subsection 2.1, diagrams with the power counting $\sim \alpha_s^{n+1}/\beta^n$ gives the order 10% corrections to leading order cross sections. Recently, full next-to-leading order corrections have been calculated for $e^+e^- \to t\bar{t}$ [22, 23, 15], and also some of the second order corrections are available [21].

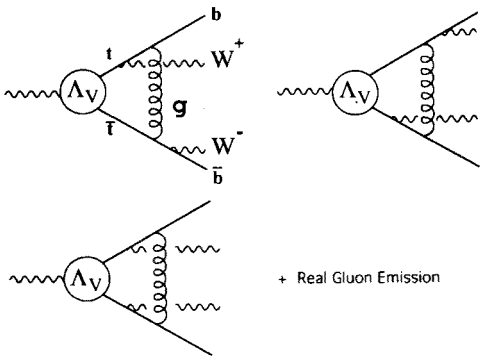

Fig. 11. Diagrams representing the final state interactions, where the gluon is exchanged between $t(\bar{t})$ and $\bar{b}(b)$ and between b and $\bar{b}$.

In addition to the same corrections which were calculated for bottomonium and charmonium, there appear corrections that are relevant only to toponium. For example, the final state interaction diagrams which contribute at the next-to-leading order are shown in Fig. 11. The contribution of the final state interaction to the top quark momentum distribution can

be written as [15]

$$\frac{d\sigma^{(FI)}}{d|\boldsymbol{p}|} \propto \alpha_s \int \frac{d^3\boldsymbol{q}}{(2\pi)^3} \frac{1}{|\boldsymbol{p}-\boldsymbol{q}|^3} \mathrm{Im}\left[\tilde{G}^*(\boldsymbol{q};E)\tilde{G}(\boldsymbol{p};E)\right]. \tag{3.18}$$

As the integrand on the right-hand-side changes sign for the exchange of variables $\boldsymbol{p}$ and $\boldsymbol{q}$, the left-hand-side vanishes upon integration over $\int d^3\boldsymbol{p}$. Namely, it turns out that the corrections from the final state interactions to the total cross section vanish [22, 23, 15]:

$$\int d\sigma^{(FI)} = 0. \tag{3.19}$$

Nevertheless, final state interactions give non-trivial corrections to the top quark momentum distributions. Shown in Fig. 12 are the momentum distributions with (solid) and without (dashed) the final state interactions. The peak position of the distribution $|\boldsymbol{p}|_{\mathrm{peak}}$ is reduced about 5% due to the correction for $m_t = 150$ GeV. One sees that the final state interaction correction grows for larger energy. One can also show that this correction decreases as $\Gamma_t \to 0$ as anticipated.

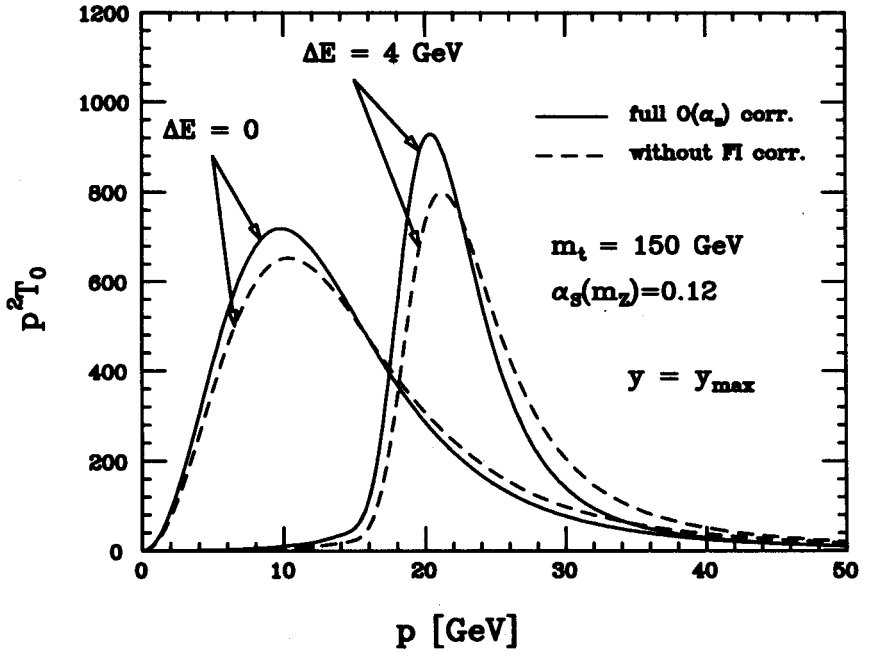

Fig. 12. The top momentum distribution $|\boldsymbol{p}|^2 T_0$ *versus* $|\boldsymbol{p}|$ with (solid) and without (dashed) the final state interaction corrections for $m_t = 150$ GeV and $\alpha_s(m_Z) = 0.12$ [15].

4. Parameter determination

In this section we list the accuracy in the determination of physical parameters which NLC has potential to achieve through the study of $t\bar{t}$ threshold cross sections. The following are the results from the quantitative studies for the sample case of $m_t = 170$ GeV, taking into account realistic experimental conditions expected at NLC [7]. The error estimates include statistical ones only.

We can measure the threshold shape by energy scan. Given 11 energy points with 1 fb^{-1} each, $\Delta m_t = 380$ MeV is expected even if α_s is totally unconstrained. On the other hand, $\Delta\alpha_s(m_Z) = 0.007$ even if m_t is unknown. The error on top width is $\Delta\Gamma_t/\Gamma_t = 0.18$ when $\alpha_s(m_Z)$ is known. For the standard model Higgs of $M_H = 100$ GeV, the Yukawa coupling can be determined with $\Delta g_{tH}/g_{tH} = 0.25$ if α_s and Γ_t are known from other sources.

The momentum spectrum measurement at $t\bar{t}$ threshold can also be used. Using the 1S peak position E_{1S} determined by the threshold scan, we can perform precision measurements of $\alpha_s(m_Z)$. $\Delta\alpha_s(m_Z) = 0.002$ is expected for 100 fb^{-1} provided E_{1S} is known. Given the same statistics, $\Delta\Gamma_t/\Gamma_t = 0.03$ if E_{1S} and $\alpha_s(m_Z)$ are known. Note that since the top momentum measurement is insensitive to the Higgs-exchange effect, the parameters determined from the top momentum measurement can be fed back to the Yukawa coupling extraction from the total cross section.

The FB-asymmetry of top quark gives additional information on α_s and Γ_t. $40k$ detected events provide us with an opportunity to measure $\alpha_s(m_Z)$ with $\Delta\alpha_s(m_Z) = 0.004$ if E_{1S} and Γ_t are known. Also, $\Delta\Gamma_t/\Gamma_t = 0.06$ if E_{1S} and $\alpha_s(m_Z)$ are known.

5. Conclusion

There appear many unique features in top quark threshold physics as compared to lighter quarkonia.

Theoretical predictions of cross sections near $t\bar{t}$ threshold are well under control. This is partly because we are reaching asymptotic region of QCD potential, and partly because the large top width acts as infrared cutoff. Full next-to-leading order corrections as well as part of the second order corrections are already available.

The $t\bar{t}$ threshold cross sections depends on physical parameters such as m_t, α_s, Γ_t, M_H, and g_{tH}. Essentially there are three independent observables that are unique to the $t\bar{t}$ threshold region. The total cross section is

[7] These are derived from the same analyses as done in Ref. [18] where the case $m_t = 150$ GeV is studied.

sensitive to the short distance physics such as Higgs-exchange effect. The top quark momentum measurement will allow to extract information on the resonance wave function, and it turns out to be most sensitive to α_s and Γ_t. The FB-asymmetry of top quark in the threshold region 'measures' the level gaps between S and P-wave resonance states, and provides another information on the physical parameters.

Although not covered in this paper, one may also perform other standard top quark measurements (top form factors, exotic decays, *etc.*) which can be done both at threshold and in open top region ($E \gg 2m_t$) [1, 24]. There seems to be some advantage of the threshold region, since the cross section is largest, and also since highly polarized top quark samples can be obtained. These remain for future study.

In conclusion, the top quark threshold is quite rich in physics, and deserves serious studies.

Most of the topics covered here are based on top quark studies in collaboration with K. Fujii, K. Hagiwara, K. Hikasa, S. Ishihara, T. Matsui, H. Murayama and C.-K. Ng. The author wishes to express his sincere gratitude to all of them. The quantitative re-analysis for $m_t = 170$ GeV case given in section 4 has been done by K. Fujii. The author is also grateful to M. Jeżabek, J. Kühn, K. Melnikov, W. Mödritsch, M. Peskin, T. Teubner, O. Yakovlev, and all the members of JLC Working Group for fruitful discussions. Finally, the author wishes to thank T. Moroi and T. Asaka for reading the manuscript carefully and making useful comments.

REFERENCES

[1] For reviews on physics that can be covered at NLC, see *Proceedings of Workshop on Physics and Experiments with Linear Colliders*, Saariselka, Finland, 11991, edited by R. Orava, P. Elrola and M. Nordbey, World Scientific, Singapore 1992; JLC Group, KEK Report 92-16 (1992); W. Bernreuther, et al., in e^+e^- *Collisions at 500 GeV: The Physics Potential, Part A, B and C*, DESY 92-123, (1992) and DESY 93-123, (1993); *Proceedings of the Workshop on Physics and Experiments with Linear* $e^+e^- \to t\bar{t}$ *Colliders*, Waikoloa, Hawaii, April 1993); K. Fujii, Talk given at 22nd INS International Symposium on Physics with High Energy Colliders, KEK preprint, 94-38, 1994.

[2] CDF Collaboration, *Phys. Rev. Lett.* **73**, 225 (1994); *Phys. Rev.* **D50**, 2966 (1994).

[3] K. Hagiwara, S. Matsumoto, D. Haidt, C. Kim, KEK preprint, KEK-TH-375, 1994.

[4] M. Jeżabek, J. Kühn, *Phys. Rev.* **D48**, R1910 (1993), and references therein.

[5] K. Hagiwara, K. Kato, A.D. Martin, C.-K. Ng, *Nucl. Phys.* **B344**, 1 (1990).

[6] J.H. Kühn, P.M. Zerwas, *Phys. Rep.* **167**, 321 (1988).
[7] V.S. Fadin, V.A. Khoze, *JETP Lett.* **46**, 525 (1987); *Sov. J. Nucl. Phys.* **48**, 309 (1988).
[8] M. Strassler, M. Peskin, *Phys. Rev.* **D43**, 1500 (1991).
[9] Y. Sumino, K. Fujii, K. Hagiwara, H. Murayama, C.-K. Ng, *Phys. Rev.* **D47**, 56 (1993).
[10] M. Jeżabek, J. Kühn, T. Teubner, *Z. Phys.* **C56**, 653 (1992); M. Jeżabek, T. Teubner, *Z. Phys.* **C59**, 669 (1993).
[11] H. Murayama, Y. Sumino, *Phys. Rev.* **D47**, 82 (1993).
[12] M. Braun, *Sov. Phys. JETP* **27**, 652 (1968).
[13] T. Appelquist, H. Politzer, *Phys. Rev. Lett.* **34**, 43 (1975); *Phys. Rev.* **D12**, 1404 (1975).
[14] G. Bodwin, D. Yennie, *Phys. Rep.* **43**, 267 (1978); see also Ref. [15].
[15] Y. Sumino, Ph. D. Thesis, Univ. of Tokyo preprint, UT-655 (1993); Y. Sumino, K. Hikasa, S. Ishihara, in preparation.
[16] K. Fujii, private communication.
[17] K. Fujii, private communication. The program used for the calculation was made originally by Z. Hioki.
[18] K. Fujii, T. Matsui, Y. Sumino, *Phys. Rev.* **D50**, 4341 (1994).
[19] P. Igo-Kemenes, M. Martinez, R. Miquel, S. Orteu, Talk given at the Workshop on Physics and Experiments with Linear e^+e^- Colliders, Waikoloa, Hawaii, April 1993.
[20] M. Jeżabek, J. Kühn, *Phys. Lett.* **B316**, 360 (1993).
[21] W. Mödritsch, W. Kummer, Universität Wien preprint, TUW-94-06, (1994); W. Kummer, W. Mödritsch, TUW-94-14, (1994).
[22] K. Melnikov, O. Yakovlev, *Phys. Lett.* **B324**, 217 (1994).
[23] V. Fadin, V. Khoze, A. Martin, *Phys. Rev.* **D49**, 2247 (1994); *Phys. Lett.* **B320**, 141 (1994).
[24] M. Jeżabek, Talk given at Zeuthen Workshop on Elementary Particle Theory: Physics at LEP200 and Beyond, Teupitz, Germany, April 1994, Universität Karlsruhe preprint, TTP-94-09.